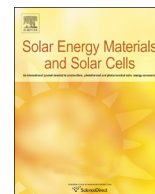




ELSEVIER

Contents lists available at ScienceDirect

Solar Energy Materials & Solar Cells

journal homepage: www.elsevier.com/locate/solmat

Diffusion of Te vacancy and interstitials of Te, Cl, O, S, P and Sb in CdTe: A density functional theory study



J.L. Roehl, S.V. Khare*

Department of Physics and Astronomy, The University of Toledo, Toledo, OH 43606, United States

ARTICLE INFO

Article history:

Received 5 September 2013

Received in revised form

6 May 2014

Accepted 28 May 2014

Keywords:

Cadmium telluride

Diffusion

Point defects

Structural properties

Energetic properties

ABSTRACT

We present an *ab initio* study of the diffusion profiles in CdTe of native, Te adatom and vacancy, and anionic non-native interstitial adatoms P, Sb, O, S, and Cl. A high symmetry Wyckoff position, 4(d) site, happens to be a global minimum energy location, *only* for O and Cl interstitials. Adatoms of P, Sb and S show an asymmetric shape of the energy diffusion barrier with two minima and two maxima in the pathway. The others, O, Cl, and Te interstitial and vacancy, show a symmetric diffusion barrier with a unique maximum and minimum. Diffusion for Te and S interstitials proceeds along the [1 1 0] channel in the crystal in a near straight line path. Diffusion for O and Cl proceeds along two nearly straight line paths along [1 1 1] and [1 1 -1]. Diffusion for P and Sb are along the [1 1 0] channel however they deviate from the straight line paths along [1 1 1] and [1 1 -1]. The rate-limiting diffusion barriers range from a low of 0.49 eV for the asymmetric diffusion path of an Sb interstitial to a high of 1.51 eV for the symmetric diffusion path of an O interstitial. The rate-limiting barriers for the others are 0.65 eV for S, 0.68 eV for both Cl and P, 1.37 eV for Te interstitial and 1.42 eV for the Te vacancy. These barriers are in agreement with the available experimental data for interstitials Te 1.40 ± 0.02 eV, Cl 0.63 ± 0.10 eV and S 0.64 ± 0.02 eV. The symmetric or asymmetric nature of the diffusion path as well as the bond length and atomic coordination at the energetic-extrema positions influence the size of the diffusion energy barrier. In addition there exist two electronic signatures in the local density of states: one for the bond breaking in the symmetric diffusion barrier paths and the other in the difference in hybridization between the global minimum and global maximum energy positions for asymmetric diffusion barriers. This work should serve as a motivation for experimental verification of other barriers and elucidates the diffusion mechanisms very difficult to discover experimentally.

© 2014 Elsevier B.V. All rights reserved.

1. Introduction

Cadmium telluride (CdTe) based thin films have emerged as the foremost technology in the growing market of thin film solar cell module production. The optimal band-gap and high photon absorption coefficient have made CdTe an excellent absorber material in thin film solar cells. Continuous advancements and the wide variety of fabrication techniques [1–6] have led to improved cell efficiencies [7] at lower costs. The ability to produce high quality CdTe layers is necessary to achieve optimal cell efficiencies. It is well known that the presence of defects in these layers, will affect the semiconductor properties [8,9] and hence overall cell efficiencies. Three types of structural defects, planar, linear and point defects, are generally considered influential [10–12]. Specifically point defects may include native defects of Cd and Te, dopants such as P or Sb, S from the cadmium sulfide (CdS)

window layer, other metal atoms such as Cu, Ag, Mo, Au depending on the back contacts used, Cl from CdCl₂ treatments, H from the heat treatments of films in hydrogen [13] and Zn, Sn, O from the transparent conducting oxides [14]. A post-deposition treatment in the presence of Cl and O₂ near 400 °C is used by essentially all research groups and manufacturers of CdS/CdTe cells and modules to reach the highest device performance. This “activation” treatment increases photocurrent and open-circuit voltage and fill factor. It has also been shown that incorporating O into the closed space sublimation growth ambient enhances CdTe device performance [15]. In addition, the activation temperatures that range from 350 °C to 450 °C provide the driving force for bulk inter-diffusion of Te and S from the CdTe and CdS layers. The diffusion of CdS, by diffusion of Cd or S, into CdTe is a faster process than that of diffusion of CdTe, by diffusion of Cd or Te, into CdS because of the heat treatment of the CdS layer prior to deposition of the CdTe layer. We have computed rate limiting diffusion barriers in CdTe of 0.33 eV [16] and 0.65 eV for interstitials of Cd and S, respectively, and rate limiting diffusion barriers in CdS [17] of 0.87 eV and 0.66 eV for interstitials of Cd and Te,

* Corresponding author. Tel.: +1 419 530 2292.

E-mail address: sanjay.khare@utoledo.edu (S.V. Khare).

respectively. This process is difficult to control, especially for cell structures with ultrathin, < 100 nm, CdS films [18], and the efficiencies of current devices are believed to be strongly dependent on this inter-diffusion at the CdS/CdTe interface [19]. Therefore, controlling defect concentration and mobility of such point defects make it important to understand the structural, energetic and electronic properties of such native and non-native point defects and their migration pathways by diffusion in CdTe. Directly elucidating such pathways experimentally in the bulk material is difficult by current techniques. On the other hand first principles computational methods are aptly suitable for this purpose [20]. However a higher requirement of computational resources and complexity has prevented much attention from being given to this problem so far. As a first step in filling this gap in the literature, we have investigated anion type defects namely Te, Cl, O, S, P and Sb in this manuscript by *ab initio* computational methods. These results can be of benefit for the understanding of CdTe/CdS technology by providing the detailed information required for a complete description of diffusion processes that is either difficult to obtain or completely unobtainable experimentally. Similarly, more extensive studies of diffusion in defected material such as at grain boundaries will provide guidance to experimental control and optimization of material properties.

2. Computational method

We have employed *ab initio* total energy calculations within the local density approximation to density-functional theory [21,22] for all computations using the Vienna *ab initio* simulation package [23–26] (VASP) suite of codes version 4.6. Core electrons are treated by ultrasoft Vanderbilt type pseudopotentials [27] as supplied by Kresse et al. [28] using the Ceperly and Alder exchange-correlation functional. A 275 eV energy cutoff was used in expanding the single-particle wave functions in the plane-wave basis. Tests using higher plane-wave energy cutoff indicated that a numerical convergence better than ± 1 meV was achieved. The lattice constant was varied and fit to a parabolic equation as a function of total energy to obtain the absolute minimum in total energy. The calculated lattice constant of 6.43 Å is within 0.5% of the experimental lattice constant [29] of 6.46 Å. A range of lattice constant values are given in Table 1. The CdTe bulk structure consists of a two-atom primitive cell zinc-blende structure (space group F-43m number 216) with the Cd and Te atoms at Wyckoff positions 4(a) and 4(c), respectively. A cubic unit cell of this zinc-blende structure consists of 8 atoms. Diffusion barrier calculations were computed in a 216 atom supercell, a $3 \times 3 \times 3$ repetition of the cubic unit cell. The larger supercell size more closely models an isolated defect by reducing the long-range interactions between defects in neighboring supercells. A Gamma point Monkhorst–Pack [30] generated k-point grid was used for the Brillouin-zone integrations in all calculations. Tests using larger

k-point sampling indicated that a numerical convergence better than ± 3 meV was achieved. All atoms were allowed to fully relax to find the minimum energy for each configuration. Relaxation was concluded when a force tolerance of 0.01 eV/Å was reached for each atom. The calculations for the local density of states (LDOS) were performed with the Gaussian smearing scheme. Diffusion barrier calculations were performed using the nudged elastic band (NEB) method [31].

3. Results and discussion

The simplest mode of diffusion in zinc-blende CdTe is interstitial diffusion down the spacious [1 1 0] channel and related symmetry equivalent directions. Interstitial diffusion down this channel consists of the diffusing adatom passing between two alternating high symmetry sites, shown in Fig. 1. The 4(b) site, Fig. 1(b), is the location of the diffusing adatom when it is tetrahedrally coordinated by Te atoms, thus labeled T_{Te} , and the 4(d) site shown in Fig. 1(c) is the location of the diffusing adatom when it is tetrahedrally coordinated by Cd atoms, thus labeled T_{Cd} . The global minimum energy site (GME) for an interstitial of Te was found to be slightly off the T_{Te} site at a distance of less than 0.30 Å, less than 11% of the 2.78 Å bulk bond length. The GME for interstitials of O and Cl was found to be at the T_{Cd} site. The GME for interstitials of P, S and Sb did not occur at either of the high symmetry sites. They occurred at a distance of greater than 1.11 Å, which is 40% of the 2.78 Å bulk bond length, from the closest high symmetry position which is the 4(b) site. For vacancy diffusion the GME was found where the bulk Te atom was removed from a 4 (c) site and the surrounding atoms were allowed to relax until convergence. Using these GME sites, as the initial and final positions, NEB runs were performed for finding the diffusion energy barriers. An odd number of images were used for symmetric barriers, and a distance of 0.5 Å was maintained between images to confirm diffusion barriers.

As the interstitial adatoms diffuse down the [1 1 0] channel, we see that different species occupy different extrema positions include the GME and both global maximum energy (GMax) and secondary maximum energy (SMax) positions, as shown in Fig. 2. These different minima and maxima positions include the GME and both globalmaximum energy (GMax) and secondary maximum energy (SMax) positions. Fig. 2 shows an example of each of the three different bonding scenarios. One scenario involves the extrema positions occurring at both of the highly symmetric Wyckoff sites. This occurs for O and Cl, where the GME and GMax positions occur at the 4(d) and 4(b) sites, respectively, where only Cl is shown in the figure. The second scenario involves only one extrema position occurring at a high symmetry site, where only the GMax of a Te interstitial occurs at the 4(d) site. The third scenario involves extrema positions that do not occur at either of the high symmetry sites. This happens for S, P and Sb, where only S is shown in the figure. The extrema positions for the Cl, Te, O, S, P and Sb interstitials are given in Table 2. Average bond lengths and angles for the configurations in Fig. 2 are given in Table 3 and the diffusion barriers for all diffusing species are given in Table 4. For a Te interstitial, the GME, Fig. 2(a), appears as a seesaw configuration with the nearest neighbor Te atoms and a square pyramidal shape formed with the closest Cd atoms. The seesaw configuration and square pyramidal can be viewed as a distorted T_{Te} site where the Te interstitial is displaced from the symmetric 4(b) position. This distortion makes interpreting values of average bond lengths and angles ambiguous. A similar situation arises for S. Hence some entries in Table 3 are not listed. The Te interstitial GMax, Fig. 2(b), occurs at the symmetric T_{Cd} position. It appears as an sp^3 hybridized tetrahedron of four Cd nearest neighbor atoms with

Table 1
Lattice parameter values.

Present work	Theoretical	Experimental
<i>Lattice constant (Å)</i>		
6.43	6.48 ^a	6.46 ^b
	6.40 ^c	
	6.43 ^d	
	6.44 ^e	

^a Theoretical values from Ref. [35].

^b Experimental values from Ref. [29].

^c Theoretical values from Ref. [36].

^d Theoretical values from Ref. [37].

^e Theoretical values from Ref. [38].

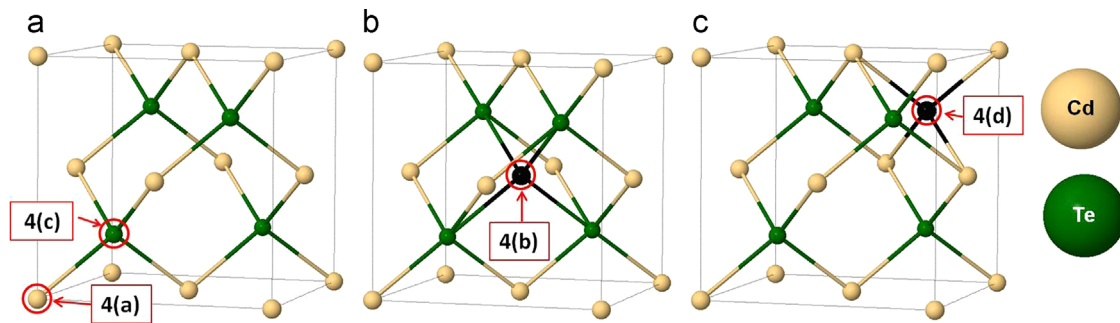


Fig. 1. Wyckoff positions for the zinc-blende CdTe crystal structure. The occupied high symmetry positions (a) are shown for the Cd bulk atom at Wyckoff position 4(a), located at the direct coordinates of the unit cell (0, 0, 0) and the Te bulk atom, Wyckoff position 4(c) located at (0.25, 0.25, 0.25). The unoccupied highly symmetric positions through which the diffusion down the [1 1 0] channel occurs are the Wyckoff position 4(b), shown in panel (b) is located at (0.5, 0.5, 0.5). We see that the 4(b) position is tetrahedrally coordinated with the bulk Te atoms. The 4(d) position, panel (c), is located at (0.75, 0.75, 0.75) and is tetrahedrally coordinated with the bulk Cd atoms.

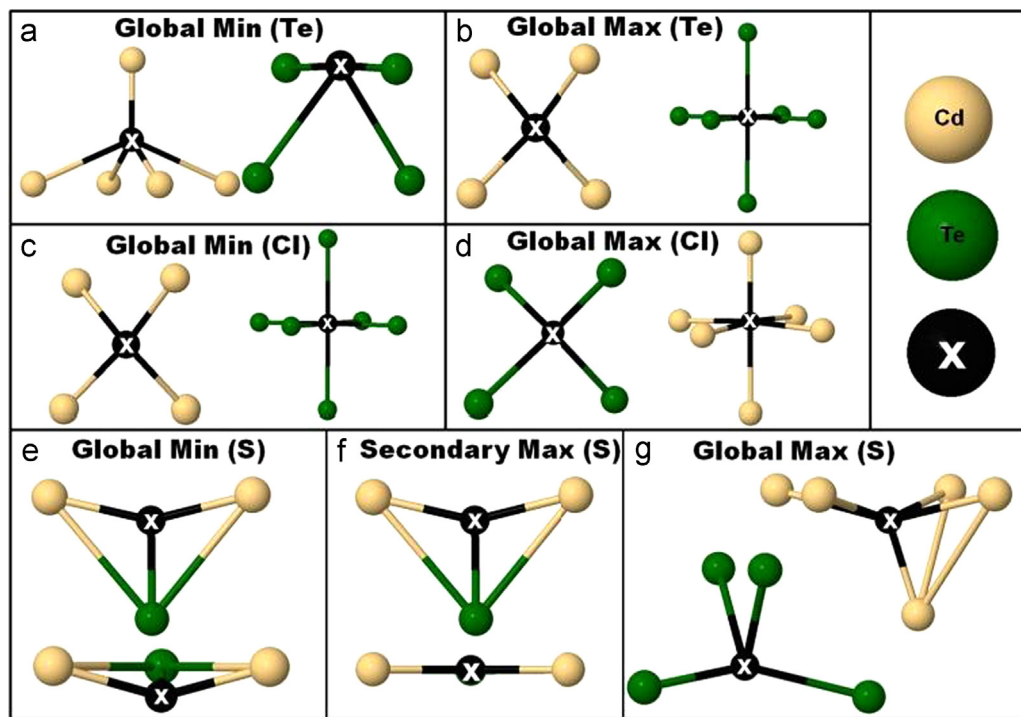


Fig. 2. Structural properties and bonding configuration of interstitial positions corresponding to various minimum and maximum energy sites. The atom labeled x is the diffusing interstitial atom, the surrounding atoms are cadmium (light yellow) and tellurium (dark green). The Te interstitial minimum energy position (a) occupies a square pyramidal site with the nearest neighbor Cd atoms and a seesaw configuration with the second shell Te atoms while the Te interstitial maximum energy position (b) is found to be at a tetrahedrally coordinated position with neighboring Cd atoms and an octahedral site with neighboring Te atoms. The minimum energy position for Cl (c) shares the same coordination as the Te interstitial at the maximum, shown in (b). The maximum position for Cl (d) reverses the coordination observed for the minimum (c). Unlike Te and Cl, the S interstitial atom encounters a second minimum energy position that is not related to the first minimum energy position by a lattice vector and encounters two in-equivalent maximums. The maximum position (f) is a flat sp^2 -like configuration consisting of two Cd and one Te atom. This is similar to the minimum energy position (e), on either side of this maximum that breaks this symmetry. The S interstitial global maximum (g) occupies a distorted Te tetrahedral position and a distorted Cd trigonal bipyramidal position. (For interpretation of the references to color in this figure legend, the reader is referred to the web version of this article.)

the Te atom in its center as seen from the average Cd–Te–Cd bond angle of 109.58° . Similarly it is octahedrally coordinated, sp^3d^2 hybridized, with the next shell of Te atoms with virtually perpendicular bond angles of 89.99° . Compared to the bulk bond lengths, the average Te–Cd bond length is 4.32% larger and the Te–Te second shell length is 25.5% smaller suggesting considerable expenditure of strain energy and hence a large energy barrier of 1.37 eV as seen in Table 4. The computed barrier of 1.37 eV is in excellent agreement with the experimental value of 1.40 ± 0.02 eV reported by Borsenberger and Stevenson [32] and Woodbury and Hall [33] for a Te interstitial.

The Cl and O interstitials occupy similar GME and GMax positions. The GME position for both Cl and O interstitial adatoms occupy the symmetric T_{Cd} position, shown for Cl in Fig. 2(c). The Cl GME makes an sp^3 -like average bond angle of 109.47° with the

four Cd nearest neighbor atoms and an sp^3d^2 -like average bond angle of 89.99° with the next shell of Te atoms. Similarly, Cl and O both occupy the same T_{Te} GMax position, shown for Cl in Fig. 2(d), where the coordination reverses and the Cl interstitial forms an sp^3 -like average bond angle of 109.27° with the four Te nearest neighbor atoms and an sp^3d^2 -like average bond angle of 89.89° with the next shell of Cd atoms. The Cl and O atoms have a nearest neighbor shell of Cd atoms in the GME in contrast to the situation in their GMax position where the first shell of atoms is of Te. This must lead to better charge transfer in the former case than in the latter thus raising the energy for the GMax site. As the Cl interstitial moves from the GME to the GMax, the Cl–Te bond length decreases 7.72% from 3.37 Å to 3.11 Å while the Cl–Cd bond length increases 13.7% from 2.70 Å to 3.07 Å. However, even though the Cl and O interstitials occupy equally coordinated

Table 2

Extrema positions given in direct coordinates, $\mathbf{R} = c_1\mathbf{a}_1 + c_2\mathbf{a}_2 + c_3\mathbf{a}_3$, of a fcc unit cell $\mathbf{a}_1 = a[0, 0.5, 0.5]$, $\mathbf{a}_2 = a[0.5, 0, 0.5]$, $\mathbf{a}_3 = a[0.5, 0.5, 0]$. For example the S minimum position is given by $\mathbf{R}[S] = 0.45\mathbf{a}_1 + 0.45\mathbf{a}_2 + 0.91\mathbf{a}_3$. The diffusion profiles for Cl, Te and O are symmetric while the diffusion profiles for S, P and Sb are asymmetric.

Element	Global min			Secondary max			Global max		
	c_1	c_2	c_3	c_1	c_2	c_3	c_1	c_2	c_3
Cl	0.75	0.75	0.75				0.49	0.57	1.45
	0.75	0.75	1.75						
Te	0.79	0.79	1.21				0.75	0.75	1.75
	0.79	0.79	2.21						
O	0.75	0.75	0.75				0.50	0.50	1.50
	0.75	0.75	1.75						
S	0.45	0.45	0.91	0.46	0.46	1.04	0.43	0.43	1.58
	0.45	0.45	1.20						
	0.45	0.45	1.91						
P	0.61	0.61	0.61	0.43	0.43	1.07	0.70	0.70	1.30
	0.61	0.61	1.17						
	0.61	0.61	1.61						
Sb	0.60	0.60	0.60	0.72	0.72	0.78	0.57	0.57	1.43
	0.60	0.60	1.21						
	0.60	0.60	1.60						

Table 3

Average bond length and angle from interstitial defect to the first two shells of neighbors which are either only Te atoms or only Cd atoms.

Element	Position	Fig. 2	Nearest-neighbor	Avg. bond length (Å)	Avg. bond angle (deg)
Te	Global Min	a	Te	–	–
	Global Max	b	Cd	–	–
			Te	3.39	89.99
			Cd	2.90	109.58
Cl	Global Min	c	Te	3.37	89.99
	Global Max	d	Cd	2.70	109.47
			Te	3.11	109.27
			Cd	3.07	89.89
S	Global Min	e	Te	2.38	–
	Secondary Max	f	Cd	2.51	137.2
			Te	2.36	–
	Global Max	g	Cd	2.52	153.3
			Te	3.08	–
			Cd	3.20	–

Table 4

Diffusion barriers (eV) for different point defects.

Element	Secondary max (eV)	Global max (eV)
Cl	–	0.68 (0.63 ^a)
O	–	1.51
S	0.07	0.65 (0.64 ^b)
Te ^v	–	1.42
Te ^l	–	1.37 (1.38 ^{c,d} –1.42 ^{c,d})
P	0.21	0.68
Sb	0.34	0.49

^a Experimental values from Ref. [34].

^b Experimental values from Ref. [19].

^c Experimental values from Ref. [32].

^d Experimental values from Ref. [33].

GME and GMax positions, as the O interstitial moves from the GME to the GMax position, the O–Te bond length decreases 24.9% from 3.42 Å to 2.57 Å while the O–Cd bond length significantly increases 49.1% from 2.22 Å to 3.31 Å. This substantial disparity in change of bond length can explain the higher diffusion barrier for

O of 1.51 eV compared to that of Cl of 0.68 eV. The 0.68 eV barrier reported here agrees well with one of the four values corresponding to diffusion profile D_{04} of 0.63 ± 0.10 eV reported by Jones et al. [34]. The D_{04} diffusion profile was obtained from the concentration profile observed at the greatest CdTe sample depth, greater than 1.5 μm.

Unlike the Te, Cl and O interstitials, the GMEs for S, P and Sb are located away from the high symmetry 4(b) and 4(d) sites. The S GMEs, Fig. 2(e), is extremely close and on either side of the SMax position, Fig. 2(f), and is similar to the sp^2 -like SMax configuration, as evidenced by the change in the S–Te and S–Cd bond lengths and bond angles. As the S interstitial moves from the GME to the SMax position, the S–Te bond length decreases only 0.84% from 2.38 Å to 2.36 Å while the S–Cd bond length increases only 0.40% from 2.51 Å to 2.52 Å and the Cd–S–Cd bond angle changes from 137.2° to 153.3°; since there is only one Te atom in this configuration, there is no listing for this value in Table 3. This is not surprising as the energy difference between these two sites is merely 0.07 eV as seen in Table 4. Decreasing the distance between images increases the resolution of the energy barrier along the diffusing path. For the S interstitial, an additional run was performed to verify the proximity of the extrema positions that maintained a distance of less than 0.3 Å between images. For the S GMEs, the S interstitial no longer lies in the plane with the two Cd and one Te atom. The S interstitial GMax, Fig. 2(g), is located at a distorted T_{Te} position and a distorted trigonal bipyramidal position with the nearest-neighbor Cd atoms. At the S GMax position, although the S–Te bond length increases 29.4% from 2.38 Å to 3.08 Å from the GME and the S–Cd bond length increases 27.5% from 2.51 Å to 3.20 Å, the Te coordination changes from 1 to 4 and the Cd coordination changes from 2 to 5. Despite this betterment in coordination the strain energy of the increased bond lengths causes a significant rise in the energy of the GMax site of 0.65 eV. The 0.65 eV barrier for S agrees well with the derived experimental value of 0.64 ± 0.01 eV for the diffusion barrier found deep in bulk CdTe by Lane et al. [19]. The increase in coordination and difference in symmetry of diffusion paths between the other group VI elements explain why the 0.65 eV barrier for S is considerably lower than the 1.37 eV and 1.51 eV barriers for Te and O, respectively. The group V elements, P and Sb, both display an asymmetric diffusion profile as mentioned. Here, we comment on the relationship between the relative change in bond length, or strain, between the extrema positions and the corresponding change in barrier energy. As the P interstitial moves from the GME to the GMax position, the P–Te bond length increases 17.8% from 2.69 Å to 3.17 Å while the P–Cd bond length increases 23.1% from 2.86 Å to 3.52 Å, resulting in a rate-limiting global diffusion barrier of 0.68 eV. As the Sb interstitial moves from the GME to the GMax position, the Sb–Te bond length increases 5.78% from 2.90 Å to 3.07 Å while the Sb–Cd bond length increases 12.5% from 2.95 Å to 3.31 Å resulting in a global diffusion barrier of 0.49 eV. The larger change in bond length for P again corresponds to a larger diffusion barrier compared to that of Sb. Also, as the Sb interstitial moves from the GME to the SMax position, the Sb–Te bond length increases 12.5% from 2.90 Å to 3.26 Å while the Sb–Cd bond length increases 2.37% from 2.95 Å to 3.02 Å resulting in a barrier of 0.34 eV. We can see that this similar change in bond length for Sb between the GME and the SMax and GMax position results in a similar diffusion barrier at both positions.

The GME for each of the interstitials Cl and O is located at the highly symmetric 4(d) site with only one GMax occurring at the other complementary high symmetry site 4(b). The symmetry of the zinc-blende crystal structure dictates that the diffusion path down the $[1\ 1\ 0]$ channel will be symmetric for these atoms. Similarly, the Te interstitial GME is located at a distorted 4 (b) site with a single GMax occurring at the 4(d) site again leading

to a symmetric diffusion path. For P, Sb and S, the GME is not located at either of the 4(b) or 4(d) sites and as a result their diffusion path is asymmetric. Furthermore, they have an additional GME, a Smax and a GMax. The first and second GME are related by a lattice vector and hence are equivalent sites, the additional GME is not related to the first or second by a lattice vector and as such P, Sb and S possess two distinct GME whereas Te, O and Cl possess only one distinct GME. This is because the GME for P, Sb and S do not occur at either of the 4(d) or 4(b) sites and symmetry of the zinc-blende structure along the $[1\ 1\ 0]$ channel requires this additional GME. The additional GMEs for P, Sb and S and the different symmetries of the diffusion paths are clearly seen in

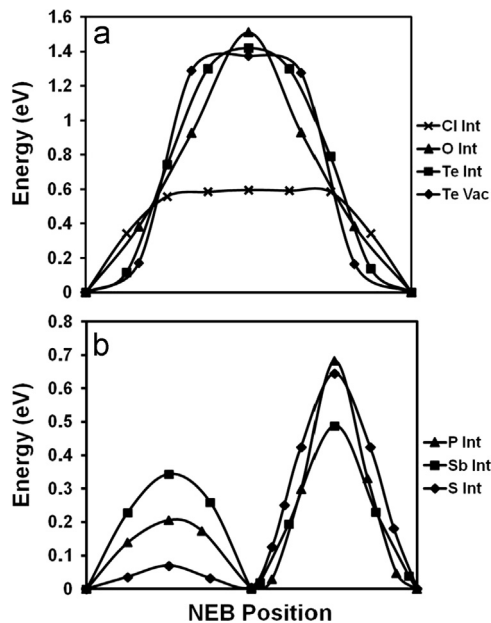


Fig. 3. NEB graphs of diffusion barrier profiles as a function of the NEB step positions, (a) the symmetric barriers (*i.e.* Cl, O and Te) and (b) the asymmetric barriers of P, Sb and S observed in CdTe. The first and last NEB positions on the x axis are displaced through a lattice vector $a[0.5\ 0.5\ 0]$ down the $[1\ 1\ 0]$ channel, where a is the computed lattice constant 6.43 Å, and hence have identical energies.

Fig. 3 for all the interstitials. We observed that both Cl and O pass directly between the two alternating 4(b) and 4(d) sites resulting in a diffusion path down the $[1\ 1\ 0]$ channel that involves alternating linear paths down along the $[1\ 1\ -1]$ direction then back up along the $[1\ 1\ 1]$ direction. This sawtooth diffusion character for O is shown in Fig. 4. In contrast, the Te interstitial GMax passes through the 4(d) position but the global minimum avoids the 4(b) position resulting in a more linear path down the $[1\ 1\ 0]$ channel, also shown in Fig. 4.

The z -axis deviation in linearity while diffusing down the $[1\ 1\ 0]$ channel is shown for all interstitials in Fig. 5. As we see from Fig. 5, the largest deviation in the z -axis is for the symmetric diffusing interstitials O, deviating approximately 0.25 Å from the O GME z -axis coordinate, followed by Cl that deviates around 0.20 Å from the Cl GME. This is expected as the O and Cl interstitials travel in the sawtooth pattern between the 4(b) and 4(d) sites. We see the previously mentioned symmetric and linear diffusion character of Te interstitial deviates less than 0.05 Å from the Te GME z -axis coordinate traveling in an almost straight line path down the $[1\ 1\ 0]$ channel. The S interstitial experiences the least deviation from the z -axis coordinate of its GME. Although the diffusion profile of S is asymmetric, the S interstitial deviates less than 0.02 Å from any GME when passing through the SMax and GMax position. The asymmetric diffusion profiles of P and Sb are quite different. The P and Sb interstitial both experience the largest deviation, greater than 0.15 Å and 0.10 Å, respectively, from their GME z -axis coordinates at the SMax position while they experience their smallest z -axis deviation, around 0.10 Å and less than 0.05 Å, respectively, at the GMax position. In addition to their similarity in z -axis deviation, both group V elements P and Sb have similar diffusion barriers. The SMax energy barriers for P and Sb are 0.21 eV and 0.34 eV with GMax energy barriers of 0.68 eV and 0.49 eV, respectively.

To further explore the relative importance of this z -axis deviation during the diffusion path we focused attention on the symmetric diffusing O and Te interstitials which show the highest and lowest z -axis deviations in Fig. 5. We performed two additional runs each for a Te and O interstitial to assess the effect of z -axis deviation on local strain energy and relaxation during diffusion. In both runs the interstitial was kept fixed with its x

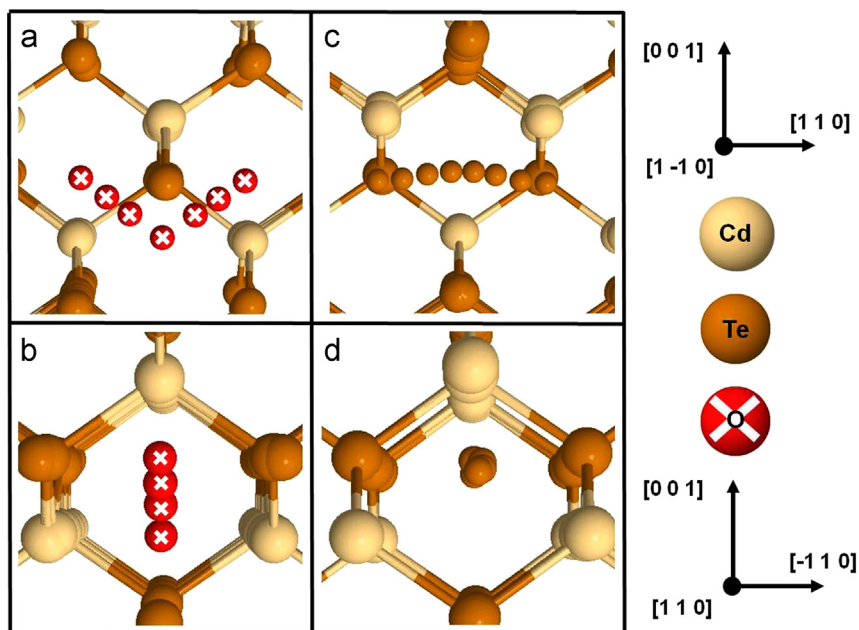


Fig. 4. Differences in diffusing paths for (a), (b) O and (c), (d) Te interstitial atoms down the $[1\ 1\ 0]$ channel in CdTe. Atoms Cl, P, and Sb have paths similar to O while S has a path similar to Te.

and y coordinates obtained from the fully converged NEB run and all other atoms in the supercell were fixed (*i.e.* unrelaxed) at their bulk equilibrium positions. The z -coordinate of the interstitial was chosen to be zero in the first, “straight line” run, while it was chosen to be the same as the one in the fully converged NEB run in the second, “bulk” run. For a Te interstitial, in Fig. 6(a), we see that the maximum strain energy occurs at the GME. This can be explained by the extreme distortion of the neighboring Te and Cd atoms of the T_{Te} , shown in Fig. 2(a). This maximum strain energy occurs at the GME for both the “straight line” and “bulk” energy. As the Te interstitial moves towards the GMax position at the T_{Cd} position, we note there is little difference between “straight line” and “bulk” energy. This can be explained by the almost straight line diffusion path of the Te interstitial with little z -axis deviation. At the GMax, the Te interstitial experiences the least “bulk” and “straight line” energy of around 3 eV. For the O interstitial the situation is reversed, the maximum strain energy occurs at the GMax T_{Te} position. We also note that there is a substantial difference between the “bulk” and “straight line” energies at the maximum position for the O interstitial, around 2 eV, compared to the difference for the Te interstitial case where the difference is negligible. This can again be explained by the character of the diffusion path. For O, the diffusion path is a seesaw pattern that experiences the largest z -axis deviation and hence largest deviation from the straight line path. We also note that the “bulk” energy for the O interstitial at the GMax is similar to the barrier energy at the same position, which can be explained because the O interstitial occupies a highly symmetric, undistorted T_{Te} position, unlike the Te interstitial GME.

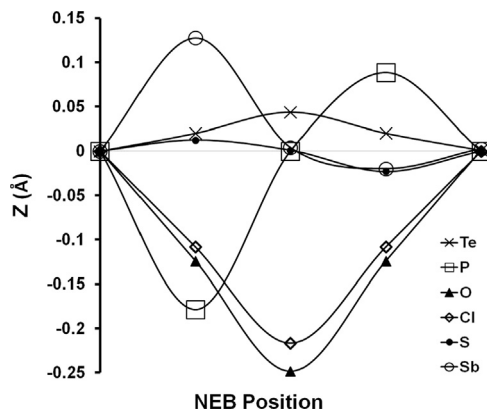


Fig. 5. The z -axis deviation from the minimum of the interstitial atoms while diffusing between global minima in adjacent unit cells down the $[1\ 1\ 0]$ channel. The ordinate axis is defined to be zero at the z -axis position of the diffusing atom in its global minimum energy site.

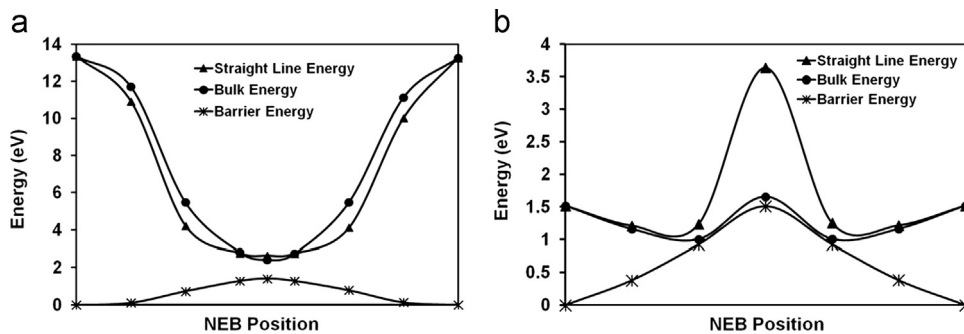


Fig. 6. Effect of local strain energy and relaxation on diffusing interstitial Te (a) and O (b) atoms. The barrier energy represents the fully relaxed diffusion barrier energy as a function of the NEB position along the diffusing path; the bulk energy is the energy of the interstitial located at the relaxed NEB position in an un-relaxed bulk cell, *i.e.* the remaining atoms are left unrelaxed in their bulk positions; the straight line energy is the energy of the NEB positions located at the same z -axis position as the minimum energy position in an un-relaxed bulk cell.

It is interesting to investigate the local density of states at the extreme positions and try to relate these electronic properties to the structural and energetic properties of the diffusing adatom along the migration path, and *ab initio* methods are able to provide information about these non-equilibrium positions that is difficult, if not impossible to access experimentally. These results are intended to complement experimental work with novel information related to the diffusion process. We computed the electronic local density of states (LDOS) of a variety of configurations of all diffusing species studied. We highlight a few observations from these computations here. An example of a symmetric diffusion barrier is illustrated in Fig. 7. It shows the LDOS for the diffusion of a Cl interstitial as it moves from the GME at the T_{Cd} site to the GMax at the T_{Te} position. The Cl interstitial at the GME position, the white atom marked ‘A’ in Fig. 7(a), is octahedrally coordinated to Te. The global maximum position, marked ‘B’ in Fig. 7(a), is tetrahedrally coordinated to Te. The black filled circles show nearest neighbor Te atoms and the nearest Cd atoms are not shown. At the GME ‘A’ position the Cl interstitial makes six symmetric bonds with Te atoms 1, 2 and 3 and atoms 4, 5 and 6. As the Cl interstitial moves from the GME ‘A’ position to the GMax ‘B’ position we clearly see that the three bonds with Te atoms 1, 2 and 3 must be broken while the bonds with Te atoms 4, 5 and 6 remain intact. Panels (b) and (c) in Fig. 7 show the LDOS for the p orbitals of the Cl interstitial and the p orbitals for its nearest neighbor Te atoms 1, 2 and 3 in (b) and for Te atoms 4, 5 and 6 in (c). We see that the substantial p - p bonding peak, around -0.3 eV, is similar in panels (b) and (c) which is expected due to the symmetric nature of the bonding at the 4(d) position. After the Cl interstitial has moved to the GMax position, we see that the p - p bonding between (e) the Cl interstitial and Te atoms 4, 5 and 6 remain and have been shifted toward the Fermi energy. However, the p - p bonding between (d) the Cl interstitial and Te atoms 1, 2 and 3 has been broken and the p states of Te atoms 1, 2 and 3 remain virtually unshifted.

An example of an asymmetric diffusion barrier is illustrated in Fig. 8. It shows the LDOS for an interstitial P atom at the GME and GMax position. We see that the p -states for the GME are shifted to deeper binding energies than the GMax position suggesting a more energetically favorable position at the GME. When the P interstitial is at the GMax position we can see that the p -states have split into three distinct peaks, two of which are shifted toward the Fermi to shallower binding energies. In addition to the splitting of the p -states at the GMax position we also observe that s -states and hybridized d -states contribute to the bonding character whereas at the GME position only the p -states contribute. A similar situation arises for another asymmetric diffusion barrier involving Sb, as shown in Fig. 9. In the figure we see the LDOS for an interstitial Sb atom at the GME, SMax and GMax positions.

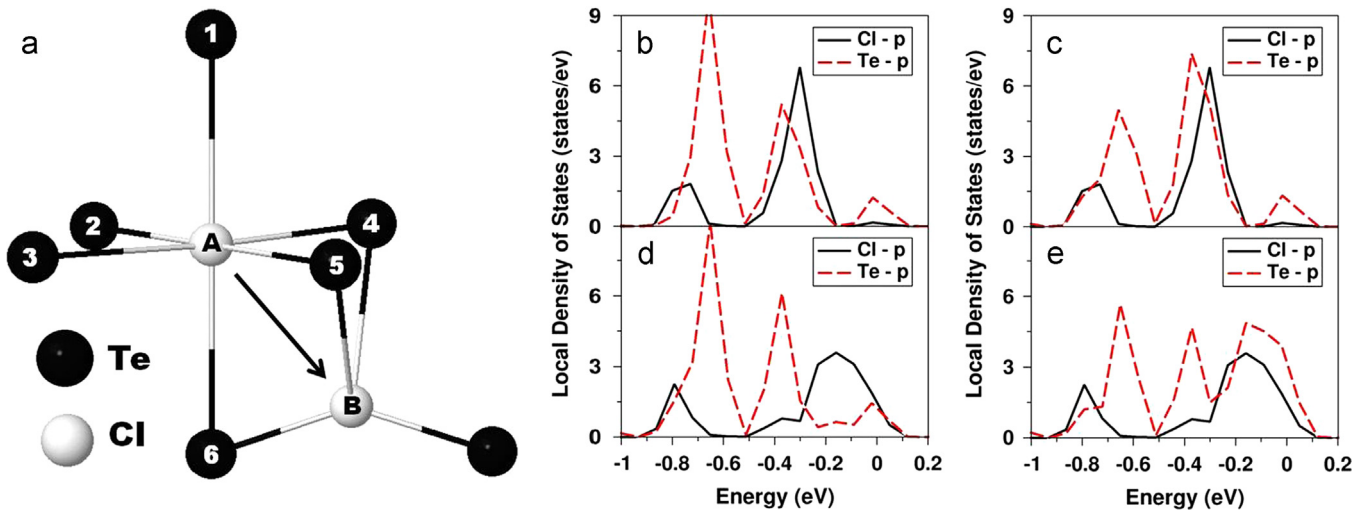


Fig. 7. Panel (a) shows the minimum energy position marked 'A' and global maximum position marked 'B' for a Cl interstitial. Filled circles show nearest neighbor Te atoms. Position A is octahedrally coordinated to Te and B is tetrahedrally coordinated to Te. Nearest Cd atoms not shown. Panels (b)–(d) show LDOS of the p orbitals of Cl interstitial and its nearest neighbor Te atoms. LDOS for Cl atom in position 'A' are in panels (b) and (c) while for position 'B' are in panels (d) and (e). LDOS for Te atoms 1, 2 and 3 are in panels (b) and (d) and for atoms 4, 5 and 6, are in panels (c) and (e). At position A, Cl forms similar bonds with all six Te atoms. This similarity is observed in panels (b) and (c). As the Cl interstitial moves from 'A' to 'B' there is little change in the LDOS in (d), of Te atoms 1, 2 and 3, while the Cl atom p-states are shifted toward the Fermi energy. This is accompanied by a similar shift for the p-states of Te atoms 4, 5 and 6 seen in (e) that remain bonded to the Cl interstitial throughout the diffusion process.

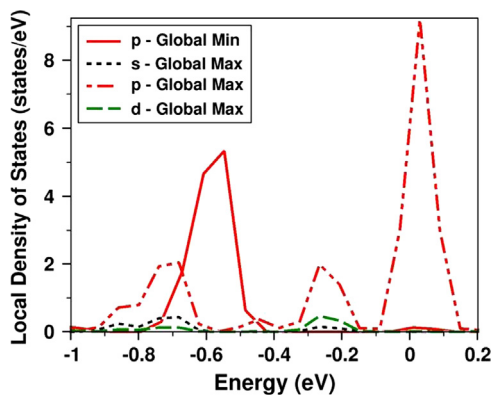


Fig. 8. LDOS by atomic orbital type (s, p, d), for an interstitial P atom, at the minimum and global maximum positions. Fermi energy is set to zero in each case. Observe the split from one peak, in the p-states, for the minimum position to three peaks for the global minimum. The overall p-state density is shifted to deeper binding energies for the minimum site. Also observe the contribution to defect states from s, p and hybridized d-states for the global maximum position and only from p-states for the minimum.

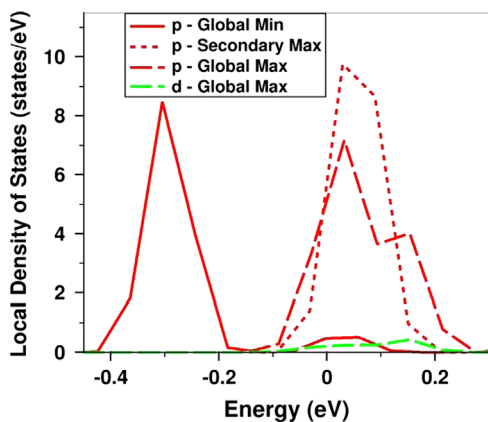


Fig. 9. LDOS of atomic orbital types, p and d, for an interstitial Sb atom at the minimum, secondary maximum and global maximum positions. Fermi energy set to zero in each case. Observe the shift to deeper binding energies for the minimum energy site and the contribution to defect states at the Fermi level from d-states for the global maximum position only.

Similar to the case for the P interstitial in Fig. 8, we see again that the p-states for the GME are shifted to deeper binding energies while the p-states for the GMax are shifted toward the Fermi to shallower binding energies. The less energetically favorable p-state shift toward the Fermi is also observed for the Sb atom at the SMax position. Similar to the case for the P interstitial in Fig. 8, we see again that hybridized d-states contribute to the bonding at the GMax position while only p-states contribute at the GME while we do not see any contribution from the s- or d-states for the Sb interstitial at the SMax position.

4. Conclusion

We have presented an *ab initio* study of the diffusion profiles in CdTe of native, Te adatom and vacancy, and anionic non-native interstitial adatoms P, Sb, O, S, and Cl. We have found that both symmetric and asymmetric diffusion paths exist. The results of this study show that the rate-limiting diffusion barriers range from a low of 0.49 eV for the asymmetric diffusion path of an Sb interstitial to a high of 1.51 eV for the symmetric diffusion path of an O interstitial. We analyzed structural motifs around the diffusing atom or vacancy through the diffusion process. The intricacies of the process were revealed through a description of the curvature of the diffusion path, relevant bond lengths, bond angles, first and second shell coordination, and local density of states. Simple predictions for other diffusing species based on our work are difficult to make. The elements belonging to a particular group do not follow any observable pattern. For example, even though Cu and Ag are in the same group 11, in the periodic table, they show very different diffusion profiles [16] where it was found that Ag had a symmetric diffusion profile and the diffusion profile of Cu and Au was asymmetric. Hence, detailed computations as presented in this manuscript are of significance. We found that the symmetric or asymmetric nature of the diffusion path as well as the bond length and atomic coordination at the energetic-extrema positions influence the size of the diffusion energy barrier. In addition we have found an electronic signature of the bond breaking in the LDOS of symmetric diffusion barriers, through the p–p bond breaking with neighboring Te atoms, as well as the difference in hybridization between the GME and GMax positions

for asymmetric diffusion barriers where s- and hybridized d-states are found to exist for only GMax positions.

Acknowledgments

The authors would like to thank the Ohio Supercomputer Center (OSC) and the National Science Foundation (NSF), USA, through Grant CNS 0855134, for providing computing resources. We thank the Wright Center for PVIC of the State of Ohio and the University of Toledo as well as the NSF (Grants CMMI 1234777, CMMI 0928440, and CMMI 0933069) for funding this work. We appreciate valuable discussions with Prof. Alvin D. Compaan.

References

- [1] J.D. Major, Y.Y. Proskuryakov, K. Durose, Impact of CdTe surface composition on doping and device performance in close space sublimation deposited CdTe solar cells, *Prog. Photovolt.: Res. Appl.* 21 (2013) 436–443.
- [2] D. Bonnet, The CdTe thin film solar cell – an overview, *Int. J. Sol. Energy* 12 (1992) 1–14.
- [3] I. Clemmink, M. Burgelman, M. Casteleyn, B.E.N. Depuydt, Screen printed and sintered CdTe–CdS solar cells, *Int. J. Sol. Energy* 12 (1992) 67–78.
- [4] S.K. Ghandhi, N.R. Taskar, I.B. Bhat, Arsenic-doped p-CdTe layers grown by organometallic vapor phase epitaxy, *Appl. Phys. Lett.* 50 (1987) 900–902.
- [5] A. Rohatgi, A study of efficiency limiting defects in polycrystalline CdTe/CdS solar cells, *Int. J. Sol. Energy* 12 (1992) 37–49.
- [6] A.D. Compaan, C.N. Tabor, L. Yuxin, F. Zhirong, A. Fischer, CdS/CdTe solar cells by RF sputtering and by laser physical vapor deposition, in: *Proceedings of 1993 Conference Record of the Twenty Third IEEE Photovoltaic Specialists Conference*, 1993, pp. 394–399.
- [7] M.A. Green, K. Emery, Y. Hishikawa, W. Warta, E.D. Dunlop, Solar cell efficiency tables (version 42), *Prog. Photovolt.: Res. Appl.* 21 (2013) 827–837.
- [8] R.W. Birkmire, B.E. McCandless, S.S. Hegedus, Effects of processing on CdTe/CdS materials and devices, *Int. J. Sol. Energy* 12 (1992) 145–154.
- [9] Y.L. Soo, S. Huang, Y.H. Kao, A.D. Compaan, Annealing effects and Te mixing in CdTe/CdS heterojunctions, *Appl. Phys. Lett.* 74 (1999) 218–220.
- [10] S.-H. Wei, S. Zhang, Chemical trends of defect formation and doping limit in II–VI semiconductors: the case of CdTe, *Phys. Rev. B* 66 (2002) 155211.
- [11] J. Britt, C. Ferekides, Thin-film CdS/CdTe solar cell with 15.8% efficiency, *Appl. Phys. Lett.* 62 (1993) 2851–2852.
- [12] K. Durose, P.R. Edwards, D.P. Halliday, Materials aspects of CdTe/CdS solar cells, *J. Cryst. Growth* 197 (1999) 733–742.
- [13] C. Ferekides, J. Britt, Y. Ma, L. Killian, High efficiency CdTe solar cells by close spaced sublimation, in: *Proceedings of 1993 Conference Record of the Twenty Third IEEE Photovoltaic Specialists Conference*, 1993, pp. 389–393.
- [14] B.E. McCandless, M.G. Engelmann, R.W. Birkmire, Interdiffusion of CdS/CdTe thin films: modeling x-ray diffraction line profiles, *J. Appl. Phys.* 89 (2001) 988–994.
- [15] W.K. Metzger, D. Albin, D. Levi, P. Sheldon, X. Li, B.M. Keyes, R.K. Ahrenkiel, Time-resolved photoluminescence studies of CdTe solar cells, *J. Appl. Phys.* 94 (2003) 3549–3555.
- [16] J.L. Roehl, S.V. Khare, Diffusion of Cd vacancy and interstitials of Cd, Cu, Ag, Au and Mo in CdTe: a first principles investigation, *Sol. Energy* 101 (2014) 245–253.
- [17] J.L. Roehl, Z.T.Y. Liu, S.V. Khare, Diffusion in CdS of Cd and S vacancies and Cu, Cd, Cl, S and Te interstitials studied with first principles computations, *Mater. Res. Express* 1 (2014) 025904.
- [18] B.E. McCandless, J.R. Sites, Cadmium telluride solar cells, in: A. Luque, S. Hegedus (Eds.), *Handbook of Photovoltaic Science and Engineering*, John Wiley & Sons, Ltd., New Jersey, 2011, pp. 600–641.
- [19] D.W. Lane, G.J. Conibeer, D.A. Wood, K.D. Rogers, P. Capper, S. Romani, S. Hearne, Sulphur diffusion in CdTe and the phase diagram of the CdS–CdTe pseudo-binary alloy, *J. Cryst. Growth* 197 (1999) 743–748.
- [20] J. Ma, S.-H. Wei, Origin of novel diffusions of Cu and Ag in semiconductors: the case of CdTe, *Phys. Rev. Lett.* 110 (2013) 235901.
- [21] P. Hohenberg, W. Kohn, Inhomogeneous electron gas, *Phys. Rev.* 136 (1964) B864–B871.
- [22] W. Kohn, L.J. Sham, Self-consistent equations including exchange and correlation effects, *Phys. Rev.* 140 (1965) A1133–A1138.
- [23] G. Kresse, J. Hafner, Abinitio molecular-dynamics for liquid-metals, *Phys. Rev. B* 47 (1993) 558–561.
- [24] G. Kresse, J. Furthmüller, Efficient iterative schemes for ab initio total-energy calculations using a plane-wave basis set, *Phys. Rev. B* 54 (1996) 11169.
- [25] G. Kresse, J. Furthmüller, Efficiency of ab-initio total energy calculations for metals and semiconductors using a plane-wave basis set, *Comput. Mater. Sci.* 6 (1996) 15–50.
- [26] G. Kresse, Technische Universität Wien, 1993.
- [27] D. Vanderbilt, Soft self-consistent pseudopotentials in a generalized eigenvalue formalism, *Phys. Rev. B* 41 (1990) 7892–7895.
- [28] G. Kresse, J. Hafner, Norm-conserving and ultrasoft pseudopotentials for first-row and transition elements, *J. Phys.: Condens. Matter* 6 (1994) 8245–8257.
- [29] O. Madelung, *Semiconductors: Data Handbook*, Springer Verlag, Berlin, 2004.
- [30] H.J. Monkhorst, J.D. Pack, Special points for Brillouin-zone integrations, *Phys. Rev. B* 13 (1976) 5188.
- [31] G. Mills, H. Jónsson, Quantum and thermal effects in H₂ dissociative adsorption: evaluation of free energy barriers in multidimensional quantum systems, *Phys. Rev. Lett.* 72 (1994) 1124–1127.
- [32] P.M. Borsenberger, D.A. Stevenson, Self-diffusion of cadmium and tellurium in cadmium telluride, *J. Phys. Chem. Solids* 29 (1968) 1277–1286.
- [33] H.H. Woodbury, R.B. Hall, Diffusion of the chalcogens in the II–VI compounds, *Phys. Rev.* 157 (1967) 641–655.
- [34] E.D. Jones, J. Malzbender, J.B. Mullins, N. Shaw, The diffusion of Cl into CdTe, *J. Phys.: Condens. Matter* 6 (1994) 7499–7504.
- [35] E. Deligoz, K. Colakoglu, Y. Ciftci, Elastic, electronic, and lattice dynamical properties of CdS, CdSe, and CdTe, *Phys. B: Phys. Condens. Matter* 373 (2006) 124–130.
- [36] O. Zakharov, A. Rubio, X. Blase, M.L. Cohen, S.G. Louie, Quasiparticle band structures of six II–VI compounds: ZnS, ZnSe, ZnTe, CdS, CdSe, and CdTe, *Phys. Rev. B* 50 (1994) 10780–10787.
- [37] M.B. Kanoun, W. Sekkal, H. Aourag, G. Merad, Molecular-dynamics study of the structural, elastic and thermodynamic properties of cadmium telluride, *Phys. Lett. A* 272 (2000) 113–118.
- [38] S.-H. Wei, S.B. Zhang, Structure stability and carrier localization in CdX (X=S, Se, Te) semiconductors, *Phys. Rev. B* 62 (2000) 6944–6947.